Volume 10
Number 4
28 January 2022
Pages 1601–2136

Journal of Materials Chemistry A

Materials for energy and sustainability

rsc.li/materials-a

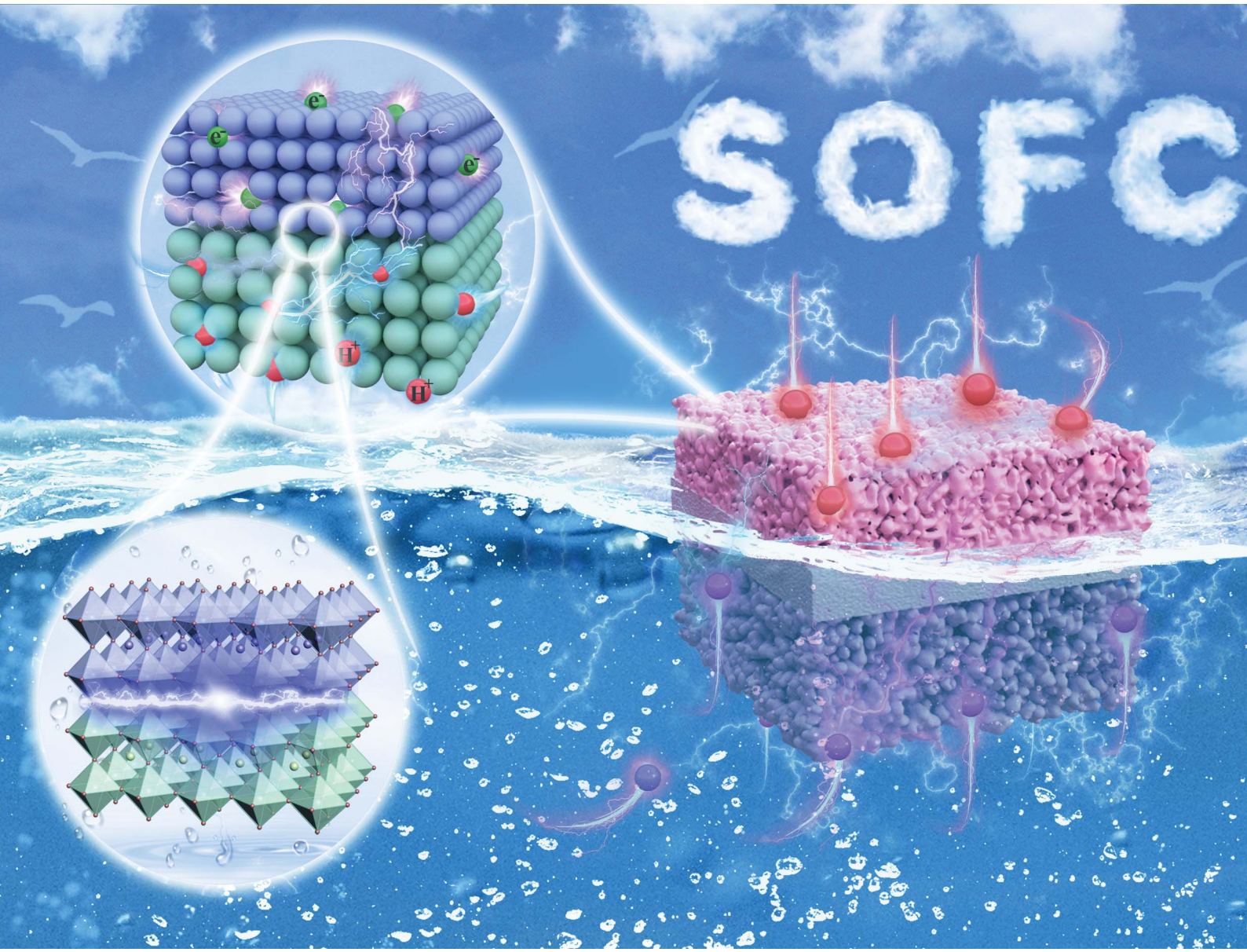

ISSN 2050-7488

ROYAL SOCIETY OF CHEMISTRY

COMMUNICATION

Lei Bi *et al.*

Triggering interfacial activity of the traditional $La_{0.5}Sr_{0.5}MnO_3$ cathode with Co-doping for proton-conducting solid oxide fuel cells

Journal of Materials Chemistry A

ROYAL SOCIETY OF CHEMISTRY

COMMUNICATION

View Article Online
View Journal | View Issue

Cite this: J. Mater. Chem. A, 2022, 10, 1726

Received 3rd November 2021
Accepted 8th December 2021

DOI: 10.1039/d1ta09450e

rsc.li/materials-a

Triggering interfacial activity of the traditional $La_{0.5}Sr_{0.5}MnO_3$ cathode with Co-doping for proton-conducting solid oxide fuel cells†

Yanru Yin,[a] Shoufu Yu,[a] Hailu Dai[b] and Lei Bi *[a]

Doping the $La_{0.5}Sr_{0.5}MnO_{3-\delta}$ (LSM) cathode with the Co element allows the new material $La_{0.5}Sr_{0.5}Mn_{0.9}Co_{0.1}O_{3-\delta}$ (LSMCo) to show improved performance compared with the Co-free LSM for proton-conducting solid oxide fuel cells (H-SOFCs), demonstrated by both experiments and first-principles calculations. More importantly, doping Co into LSM triggers the activity of the cathode/electrolyte interface in the composite cathode, leading to an impressively high fuel cell performance of the cell using the LSMCo composite cathode and also revealing the importance of the interfacial design for the cathode of H-SOFCs.

Sustainable development of the current world requires the exploration of new and efficient technologies for energy conversion.[1–5] Solid oxide fuel cells (SOFCs) can directly convert chemical energy into electricity, and they are an essential member of the family of renewable and sustainable technologies.[6,7] Although traditional SOFCs show sufficient power output for commercial applications, their high working temperatures (above 800 °C) impose some problems, such as reducing the cell's lifetime and increasing the cost of compatible materials. Therefore, the reduction of the working temperature for SOFCs is a hot topic in the research field of SOFCs.[8] Compared with intermediate temperature SOFCs using an oxygen-ion conducting electrolyte, proton-conducting SOFCs (H-SOFCs) in which proton-conducting oxides are used as the electrolyte offer the advantage of no dilution of fuels under the operation conditions.[9,10] In addition, the high conductivity and low activation energy of the proton-conducting electrolyte compared with many of the existing oxygen-ion conducting electrolytes in principle benefit the operation at intermediate temperatures.[11–15] In the past decade, the performance of H-SOFCs has been much improved by using new electrode materials[16–18] or by optimizing the cell structures.[19–21] It has been recognized that the operation of H-SOFCs needs the development of efficient cathode materials that can show adequate performance with the decreased working temperature.[22–25]

The development of new cathode materials is the most focused area in the H-SOFC field, and some materials are reported to show high performance for H-SOFCs,[26–29] although their utilization in commercial applications needs to be further demonstrated. In contrast, Sr-doped $LaMnO_3$ (LSM) is one of the most classical cathode materials for SOFCs that has been successfully used in commercial SOFCs due to its good stability and thermal match.[30] However, LSM is almost not utilized for H-SOFCs as LSM only shows adequate performance at high temperatures (above 700 °C).[31,32] Some attempts have been made to employ LSM in H-SOFCs.[19,33,34] Even though some optimization strategies (such as inkjet printing[19] and nanofibers[33]) have been used, the performance of LSM in H-SOFCs is still not satisfactory, and is much lower than that of the newly developed high-performance cathode. It is desirable to take advantage of the high stability of LSM and improve its performance in H-SOFCs. Furthermore, the composite cathode where the electrode and the electrolyte couple to extend the triple-phase boundaries (TPBs) is widely used for H-SOFCs.[35] The introduction of the electrolyte material (proton-conducting oxides) in the composite cathode provides pathways for proton migrations. However, the interfaces of different phases sometimes give enhanced performance that has been identified in other fields (such as solar cells and secondary batteries),[36–40] implying that the interfacial activity of the composite cathode for H-SOFCs might be important. Although such an interaction has not been revealed for H-SOFC cathodes before, it would be an interesting topic to study. It is reasonable to assume that proper tailoring of the interfacial activity of composite cathodes in H-SOFCs may also influence the fuel cell performance. In this study, we proposed a Co element doping strategy to tailor the traditional LSM cathode for H-SOFCs. Besides the improvement in material's properties, the Co element doping method triggers

[a]School of Resource Environment and Safety Engineering, University of South China, Hengyang 421001, China. E-mail: lei.bi@usc.edu.cn; bilei81@gmail.com

[b]School of Materials Science and Engineering, Yancheng Institute of Technology, Yancheng 224051, China

† Electronic supplementary information (ESI) available. See DOI: 10.1039/d1ta09450e

the activity of the interface between the cathode and proton-conducting oxide phase in the composite cathode, allowing an impressive improvement in fuel cell performance.

$La_{0.5}Sr_{0.5}MnO_3$ (LSM) and $La_{0.5}Sr_{0.5}Mn_{0.9}Co_{0.1}O_3$ (LSMCo) materials were synthesized by a wet chemical route, and their phase composition is shown in Fig. 1(a) and (b). One can see that a pure structure is obtained for both LSM and LSMCo, and the peaks of LSMCo shift to higher angles, suggesting the shrinkage of the lattice of LSM after Co-doping. The lattice shrinkage is expected as the ionic radius of the Co cations (65 pm for Co^{2+} and 54.5 pm for Co^{3+}) is smaller than that of Mn cations (67 pm for Mn^{2+} and 58 pm for Mn^{3+}). The lattice shrinkage is further demonstrated with the high-resolution transmission electron microscopy (HRTEM) analysis as shown in Fig. 1(c) and (d) and the *d*-spacing value is 2.70 and 2.67 Å for LSM and LSMCo, respectively. The elemental distribution analysis shown in Fig. 1(e) indicates the homogenous distribution of Co in LSM without any observable segregation, further suggesting the incorporation of Co into LSM.

The exploration and comparison of the LSM material properties after Co-doping are carried out at the atomic level by using the density functional theory (DFT) method. The poor activity of LSM at an intermediate temperature is due to its electronic conducting nature without good ionic conductivity. It is found that the formation of oxygen vacancies (Vo), which is critical for oxygen-ion diffusion,[41] becomes easier for LSM after Co element doping, as evident from the observation that the energy for Vo formation (E_{Vo}) decreases from 2.14 eV for LSM to 1.95 eV for LSMCo. The decreased E_{Vo} results in a larger Vo content at the LSMCo surface, which is confirmed by X-ray photoelectron spectroscopy (XPS) analysis as shown in Fig. S1.† The ratio between the adsorbed O and lattice O, which reflects the content of Vo, is larger for LSMCo (0.66) than that for LSM (0.49), suggesting that a more Vo-rich surface is obtained for LSMCo.[42,43] Besides the improvement in Vo, the hydration energy (E_{hydra}), which is another important parameter of the H-SOFC cathode,[44,45] is also improved with Co doping into LSM. The calculated E_{hydra} for LSM and LSMCo is 0.19 and −0.27 eV, respectively. The value is positive for LSM and turns to be negative for LSMCo, indicating that the hydration behavior is thermodynamically unfavorable for LSM, and it becomes favorable for LSM with Co-doping. Furthermore, the proton hopping barrier from one O atom to the neighboring O atom is reduced from 0.33 eV for LSM to 0.25 eV for LSMCo, suggesting that the migration of protons in LSMCo would encounter a lower barrier compared with that in LSM and thus benefiting

Table 1 Calculated E_{Vo}, E_{hydra} and E_{migra} for LSM and LSMCo

	LSM	LSMCo
E_{Vo} (eV)	2.14	1.95
E_{hydra} (eV)	0.19	−0.27
E_{migra} (eV)	0.33	0.25

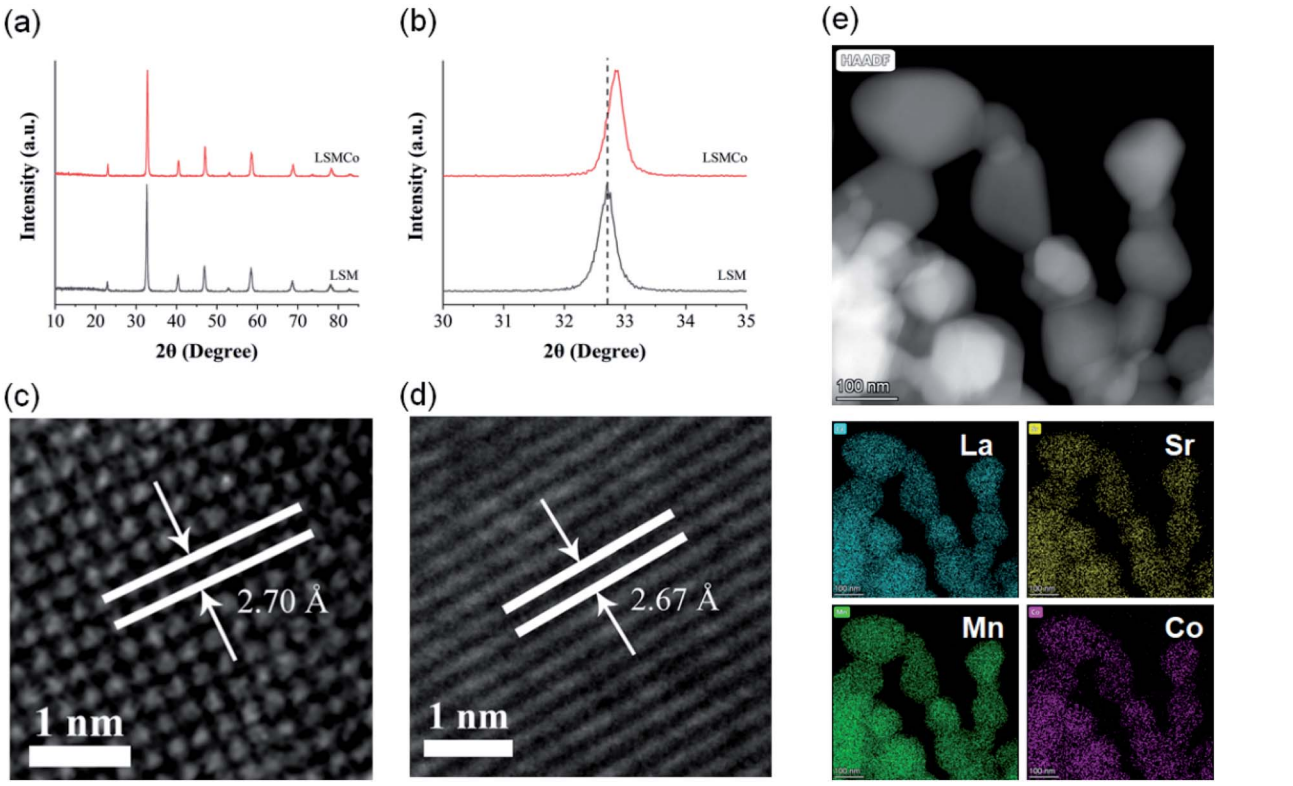

Fig. 1 (a) XRD patterns for LSM and LSMCo powders and (b) their enlarged view from 30 to 35 degree; HRTEM image for (c) LSM and (d) LSMCo; (e) HADDF-EDS for LSMCo.

its application in H-SOFCs. The E_{Vo}, E_{hydra} and migration energy (E_{migra}) for LSM and LSMCo are summarized in Table 1.

The above evidence indicates that LSMCo as a cathode in principle could deliver better performance than LSM for H-SOFCs. To validate this point, H-SOFCs using LSM and LSMCo cathodes were fabricated and tested. H-SOFCs include the NiO–BCZY composite anode, BCZY electrolyte, and LSM (or LSMCo) cathode. It should be noted that a single-phase LSM or LSMCo cathode was used for these cells. As expected, the fuel cell performance has been improved by switching the cathode from LSM to LSMCo. The cell using the LSM single-phase cathode generates a peak power density of 234, 366, and 515 mW cm^{-2} at 600, 650, and 700 °C, respectively, as shown in Fig. 2(a). In contrast, an improvement in fuel cell performance is obtained for the cell using the single-phase LSMCo cathode, reaching 302, 470, and 672 mW cm^{-2} at 600, 650, and 700 °C, respectively (Fig. 2(b)). The electrochemical impedance spectroscopy (EIS) analysis of both cells indicates that the LSM single-phase cathode shows a polarization resistance (R_p) of 0.124 Ω cm^2 at 700 °C and the R_p decreases to 0.106 Ω cm^2 for LSMCo (Fig. 2(c)). As both cells use the same anode and electrolyte and also exhibit a similar structure as shown in Fig. 2(d) and (e), different R_p values should originate from the use of different cathode materials. The results are expected as the formation of Vo, protonation and proton migration are improved with the Co doping in LSM that in principle could enhance the cathode performance in H-SOFCs. It is also interesting to find that the LSMCo cathode layer adheres well with the electrolyte layer even after fuel cell testing, without visible delamination. Although one drawback of Co-containing cathodes is the thermal mismatch with the electrolyte due to their high TEC values,[46] the LSMCo single-phase cathode can adhere well to BCZY, which implies that LSMCo possibly exhibits a compatible TEC value with the electrolyte. The thermal expansion measurement was carried out for LSMCo and the result is shown in Fig. 2(f). One can find that the thermal expansion coefficient (TEC) value of LSMCo is 13.6 × 10^{-6} K^{-1}, which is close to that of the BCZY electrolyte, being 10.1 × 10^{-6} K^{-1}.[47] In addition, the TEC value of LSMCo is almost the same as that of LSM (13.8 × 10^{-6} K^{-1}), suggesting that 10% Co-doping into LSM does not change the thermal expansion behavior of LSM and the LSMCo cathode still shows a good thermal match with the electrolyte.

Although an improved fuel cell performance can be obtained for the LSMCo cathode, the performance is still moderate compared with the recently reported high-performance cathode for H-SOFCs. It should be noted that the above study only uses the single-phase LSMCo material as the cathode without coupling it with proton-conducting oxides. Therefore, it is reasonable to predict that the performance of the composite LSMCo cathode would be further improved as the proton-conducting phase in the composite cathode could provide additional pathways for proton migrations and thus extends the triple-phase boundaries (TPBs). It should be mentioned that the proton-conducting oxide $BaZr_{0.8}Y_{0.2}O_{3-\delta}$ (BZY) instead of BCZY was used as the proton-conducting phase in the composite cathode. BZY that has poor sinterability when used in the cathode could offer more porosities in the composite cathode compared with the one using BCZY,[48] benefiting the gas diffusion at the cathode. Although the improvement in the fuel cell performance is foreseen by using the composite cathode instead of the single-phase LSMCo cathode, the enhancement in fuel cell performance is beyond expectation. Fig. 3(a) indicates that H-SOFC using the LSMCo–BZY composite cathode

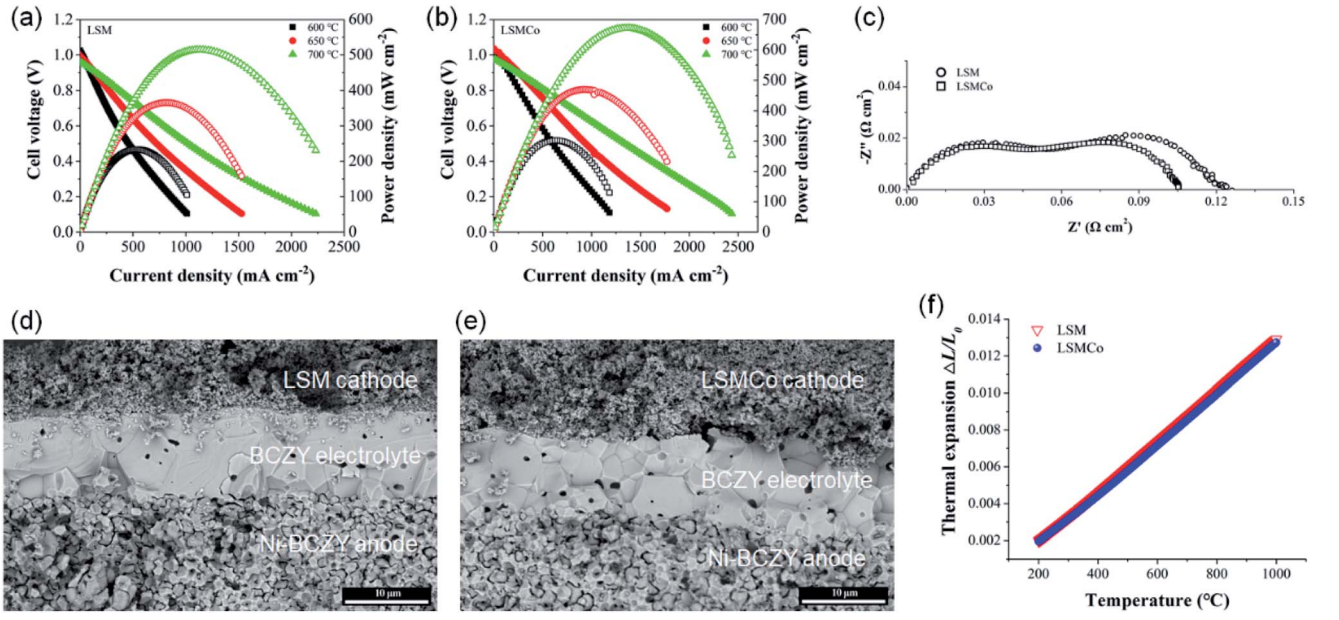

Fig. 2 *IV* and power density curves for H-SOFCs using (a) LSM single-phase cathode and (b) LSM single-phase cathode; (c) EIS plots for the cells using LSM and LSMCo single-phase cathodes; cross-sectional view for the corresponding (d) LSM cell and (e) LSMCo cell. The images are taken in the Back-Scattered Electron (BSE) mode; (f) comparison of TEC between LSM and LSMCo materials.

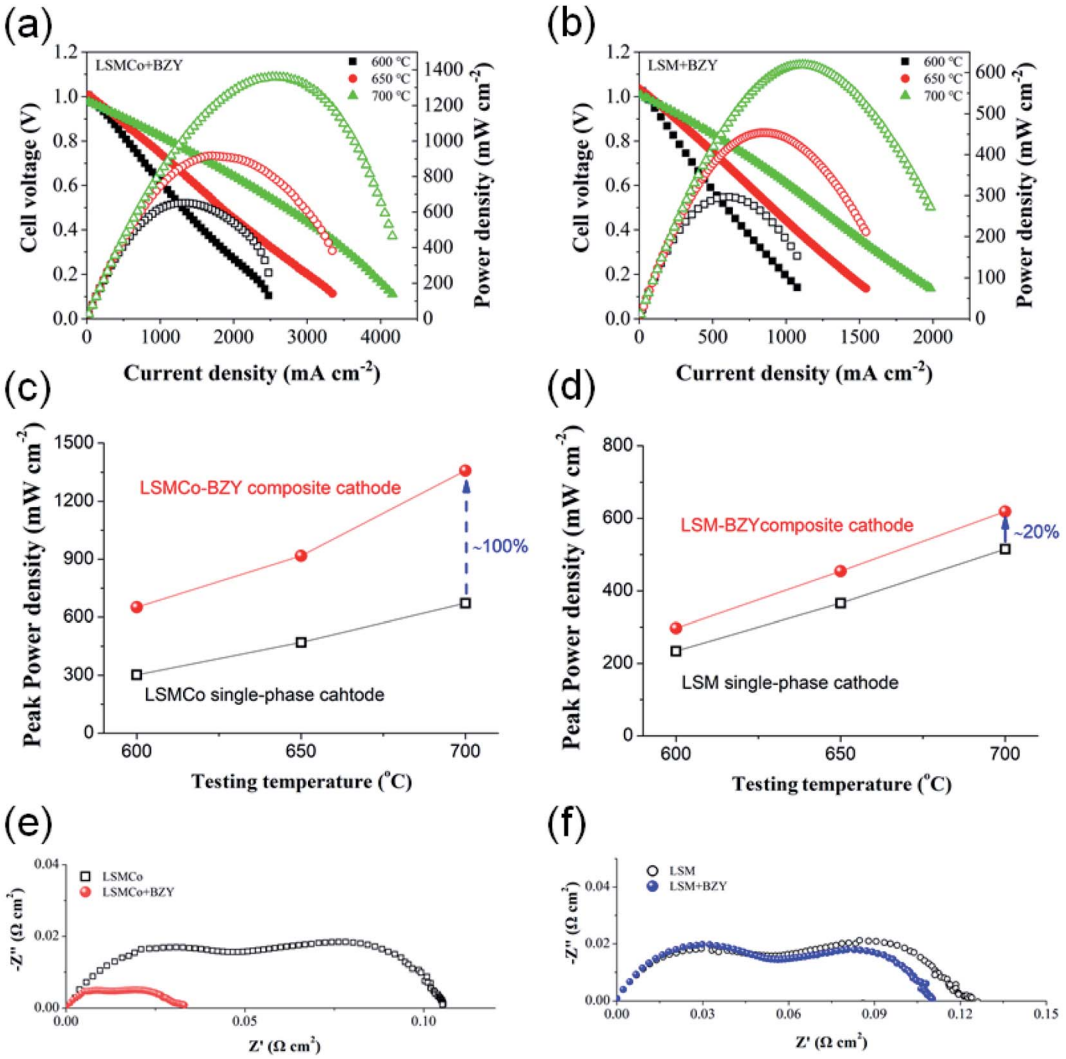

Fig. 3 *IV* and power density curves for H-SOFCs using (a) LSMCo–BZY composite cathode and (b) LSM–BZY composite cathode; comparison of peak power density between (c) LSMCo single-phase cathode and LSMCo–BZY composite cathode as well as (d) LSM single-phase cathode and LSM–BZY composite cathode; comparison of EIS plots between (e) LSMCo single-phase cathode and LSMCo–BZY composite cathode as well as (f) LSM single-phase cathode and LSM–BZY composite cathode.

shows peak power densities of 651, 917, and 1359 mW cm^{-2} at 600, 650, and 700 °C, respectively, which are significantly higher than that of the cell using the single-phase LSMCo cathode, being 302, 470, and 672 mW cm^{-2} at 600, 650, and 700 °C, respectively. In contrast, the enhancement of the cell by switching the cathode from single-phase LSM to the composite LSM–BZY cathode is much less profound, from 234, 366, and 515 mW cm^{-2} to 297, 454, and 619 mW cm^{-2} at 600, 650, and 700 °C, respectively, as shown in Fig. 3(b). The performance enhancement from LSM single-phase cathode to LSM–BZY composite cathode is about 20%, whereas the enhancement from LSMCo single-phase cathode to LSMCo–BZY composite cathode is around 100% at each testing temperature, as shown in Fig. 3(c) and (d). The EIS analysis also indicates that the decline of R_p is significant for LSMCo-based cathodes, from 0.106 Ω cm^2 for the LSMCo single-phase cathode to 0.0334 Ω cm^2 for the LSMCo–BZY composite cathode at 700 °C (Fig. 3(e)). In contrast, despite observation of the reduction in R_p for the LSM–BZY composite cathode, the decrease is only from 0.124 Ω cm^2 for the LSM single-phase cathode to 0.11 Ω cm^2 for the LSM–BZY composite cathode (Fig. 3(f)). The cross-sectional view of the LSM–BZY and LSMCo–BZY cells (Fig. S2†) indicates that both cells share similar microstructures and their microstructure is similar to that of their single-phase cathode counterpart. If the proton-conducting phase only serves as the pathway for proton migrations, the enhancement degree in performance should be similar for both the LSMCo–BZY composite cathode and LSM–BZY composite cathode, which is not the case in this study. Therefore, there must be some factors else that influence the performance of the composite cathode. The chemical compatibility between LSMCo and BZY is examined by *in situ* high-temperature XRD (HT-XRD), and the result is shown in Fig. S3.† One can find that there is no reaction between LSMCo and BZY up to 1000 °C, suggesting that the ultra-high

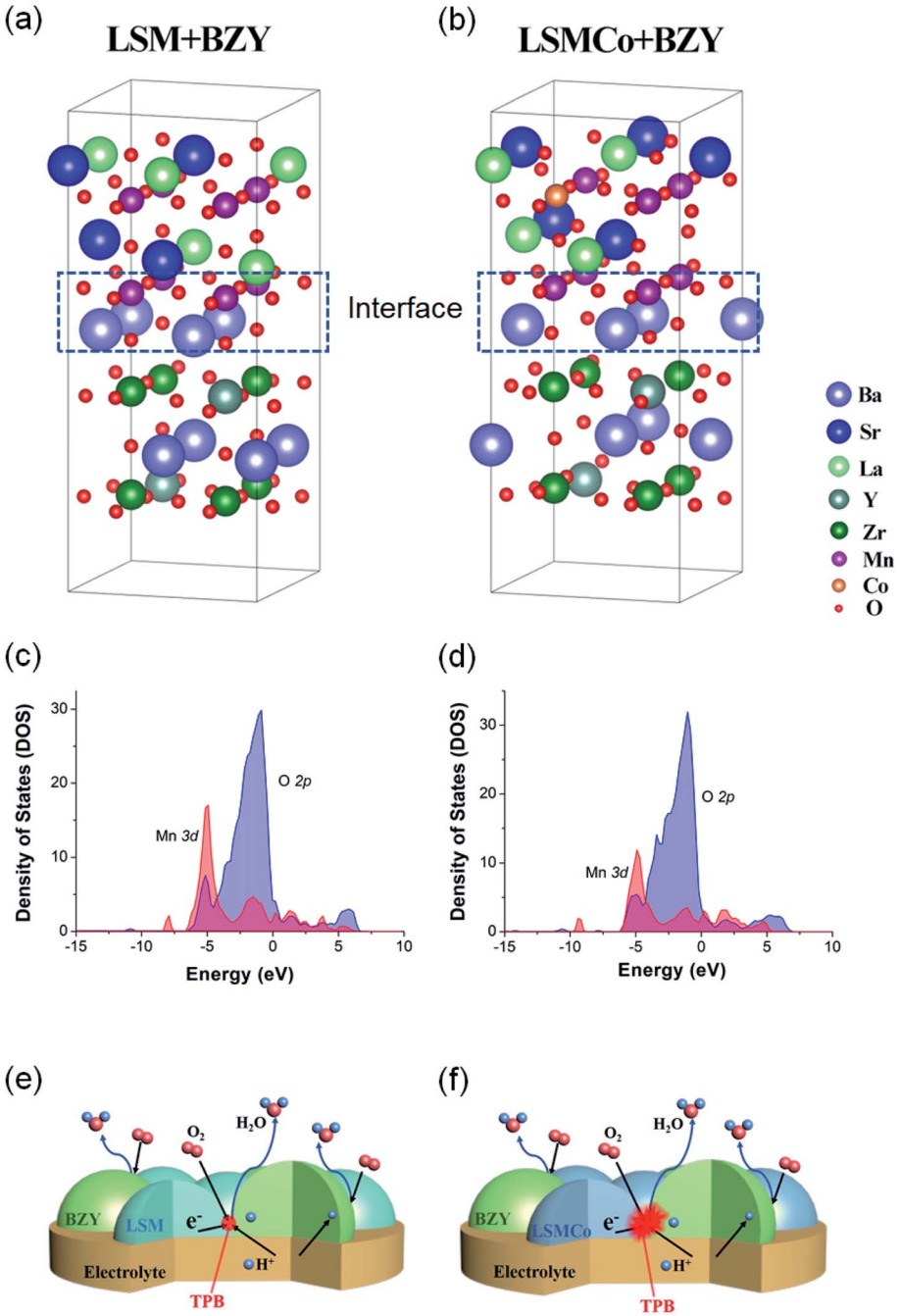

Fig. 4 DFT calculated configuration of (a) LSM/BZY and (b) LSMCo/BZY interfaces; calculated DOS of Mn 3d and O 2p orbitals for (c) LSM/BZY and (d) LSMCo/BZY; scheme of the cathode reaction at (e) LSM/BZY and (f) LSMCo/BZY, suggesting a more active TPB at the LSMCo/BZY cathode interface.

performance of LSMCo–BZY is not resulted from the formation of any new phase. Further examination was carried out to check the chemical compatibility between LSMCo and BCZY, which was used to exclude the possibility of performance enhancement from newly formed secondary phases at the cathode/electrolyte interface during the cathode/electrolyte co-firing procedure. The LSMCo + BCZY composite powder was co-fired under the cathode layer fabrication conditions (900 °C for 10 min in the microwave sintering furnace) and the phase composition after co-firing was characterized by XRD. No evident secondary phase can be found for the LSMCo + BCZY composite powder after firing (Fig. S4†), suggesting the good chemical compatibility between LSMCo and BCZY up to the cathode co-firing temperature. Therefore, it can be concluded that the dramatic enhancement in fuel cell performance is not due to the formation of new phases. It is noted that the enhancement in catalytic activity at the interface of two different phases is reported for thin films in the nano-range,[49]

although such a phenomenon is rarely reported for H-SOFCs up to now. It is reasonable to assume that the interface activity may be triggered at the LSMCo/BZY interface compared with the LSM/BZY interface. To prove this hypothesis, DFT calculations are used to analyze the properties at the LSMCo(LSM)/BZY interface, and two supercells are constructed, as shown in Fig. 4(a) and (b). The formation of oxygen vacancies is important for the catalytic activity of the cathode,[50–52] and it is interesting to find that the E_{Vo} differs greatly at the LSMCo/BZY interface and the LSM–BZY interface. DFT calculations were used to investigate the E_{Vo} at the LSMCo/BZY and LSM/BZY interfaces. When the LSMCo–BZY composite is used, the formation of oxygen vacancies becomes easier compared with that in the pure LSM, as evidenced from the reduced E_{Vo} from 2.14 eV for pure LSM to −2.76 eV at the LSMCo/BZY interface, suggesting that the oxygen atoms are activated with the construction of the LSMCo/BZY interface, and the formation of Vo is thermodynamically favorable. In contrast, the oxygen atoms at the LSM/BZY interface become more inert compared with that in the pure LSM as the E_{Vo} at the LSM/BZY interface is 4.26 eV which is even larger than that of LSM (2.14 eV), indicating that the construction of the LSM/BZY interface deactivates the oxygen atoms at the interface. XPS analysis was employed to study the oxygen species of the LSM–BZY and LSMCo–BZY composite cathodes after co-firing, and the results are shown in Fig. S5.† The ratio between the O_{ads} and O_{lat}, which reflects the content of Vo, is 0.65 for LSM–BZY and 2.13 for LSMCo–BZY, respectively. The much larger value suggests more abundant Vo for the LSMCo–BZY composite cathode compared to that for the LSM–BZY composite cathode. This result is consistent with the DFT calculations. In addition, the distance between Mn 3d and O 2p (D_{3d-2p}) decreases with the Co-doping, from 1.38 for LSM/BZY to 0.81 for LSMCo/BZY, as shown in Fig. 4(c) and (d). It has been reported that the decreased D_{3d-2p} could promote oxygen reduction reaction (ORR) ability by enhancing the charge transfer and gas adsorption and desorption.[53,54] Therefore, the reduced D_{3d-2p} coupled with the decreased E_{Vo} could be the reason for the dramatically improved performance with the LSMCo/BZY cathode compared with the traditional LSM/BZY cathode. This phenomenon indicates that the Co doping into LSM further allows high interfacial activity, benefiting SOFC applications. Of course, the introduction of the proton-conducting phase BZY in the composite cathode could extend the TPBs that could be the reason for the improved fuel cell performance of the composite cathode compared with the single-phase cathode for both LSM and LSMCo in the present study. However, the poor activity of the LSM/BZY interface balances the function of TPB extensions, making the improvement in fuel cell performance quite moderate. In contrast, besides the extension of TPBs by using the composite cathode, the incorporation of Co into LSM optimizes the interfacial activity in the composite cathode. This synergistic effect between TPB extensions and enhancement in interfacial activity could be the reason for impressively high fuel cell performance of the H-SOFCs using the LSMCo–BZY composite cathode, as shown in Fig. 4(e) and (f).

LSM-based H-SOFCs only show moderate performance in the literature reports as summarized in Table 2,[19,33,34,55–58] and the current H-SOFCs using the LSMCo–BZY cathode show the highest performance ever reported for H-SOFCs using LSM-based cathodes. The fuel cell performance is even several times higher than that of some LSM-cells in previous reports. It is noted that even though some optimization strategies have been used for LSM cathodes, the performance of LSM-based H-SOFCs in literature reports is still much lower than that of recently reported high-performance SOFCs, thus leading to the traditional thinking that this classical cathode cannot challenge the new cathode from the perspective of cell performance. However, this opinion might be turned over with the use of the LSMCo–BZY composite cathode, as it boosts the cell performance to a new record-high level among LSM-based cells. The cell performance is not only the highest ever reported for LSM-based H-SOFCs but also surpasses that of most of the H-SOFCs reported recently. Compared with the high Ba concentration in many high-performance cathodes in the literature,[19,21,42] the excellent stability of the LSM-based material makes it more attractive for practical applications. In the LSMCo–BZY composite cathode, the excellent chemical stability of BZY is well known and the good stability of LSM is also inherited by LSMCo, as evidenced in the chemical stability tests. No matter treating the LSMCo powder in a 10% CO_2-containing atmosphere at 700 °C for 10 h (Fig. 5(a) and S6†) or under steam conditions (30% H_2O) for 10 h (Fig. 5(b)), the structure of LSMCo remains stable without observable secondary phases, suggesting that the good stability of LSM is inherited by LSMCo and the LSMCo material also exhibits good chemical stability against CO_2 and H_2O. It is noted that the CO_2 concentration in air is only 0.03%, which is more than two orders of magnitude lower than that in our stability test. LSMCo, which can survive under the more severe conditions in the stability test, is expected to show sufficient stability under the cathode working conditions (air). The excellent chemical stability of the material renders good long-term stability of the material under the operation conditions. The H-SOFC using the LSMCo–BZY composite cathode works stably for more than 200 h, as shown

Table 2 Fuel cell performance of LSM-based H-SOFCs. LSM98: $(La_{0.8}Sr_{0.2})_{0.98}MnO_3$; BCY: $BaCe0_{.85}Y_{0.15}O_3$; LSM20: $La_{0.8}Sr_{0.2}MnO_3$; LSMZn: $La_{0.5}Sr_{0.5}Mn_{0.875}Zn_{0.125}O_3$

Composition	Peak power density (mW cm^{-2})	Year (ref.)
LSM98–BZY	25 (800 °C)	2008 (ref. 34)
LSM20–BCY	430 (750 °C)	2013 (ref. 55)
LSM20–BCY	580 (700 °C)	2015 (ref. 56)
LSM20–BZY[a]	200 (600 °C)	2018 (ref. 19)
LSM20–BCZY[b]	850 (700 °C)	2020 (ref. 33)
LSM–BCZY	671 (700 °C)	2021 (ref. 57)
LSMZn–BZY	1012 (700 °C)	2021 (ref. 58)
LSMCo–BZY	651 (600 °C)	This study
	1359 (700 °C)	

[a] Inkjet printing technology was employed to make nanosized LSM20 particles. [b] LSM20 nanofibers were used.

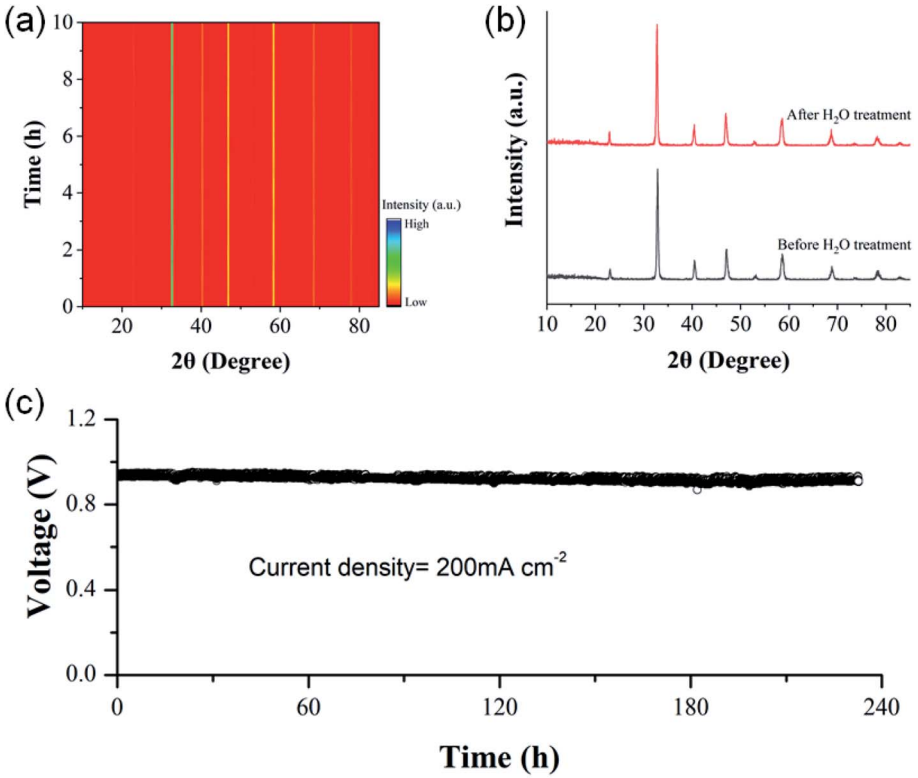

Fig. 5 (a) Time course of the *in situ* XRD patterns for LSMCo in CO_2-containing atmosphere measured at 700 °C; (b) XRD patterns for LSMCo before and after the H_2O treatment; (c) stability test for the cell with the LSMCo–BZY cathode tested at 600 °C.

in Fig. 5(c). The high performance of the LSMCo–BZY cathode for H-SOFCs is compatible with the good stability, demonstrating an efficient way to tailor and utilize the interface of the traditional LSM cathode and bringing a new life to this classical SOFC cathode for H-SOFCs.

Conclusions

LSM is the first-generation cathode and one of the most classical cathodes for SOFCs, but its pure electron-conducting nature that cannot work well at intermediate temperatures prevent its applications in H-SOFCs. Although doping the Co element into LSM can improve the performance of H-SOFCs, the enhancement is demonstrated to be still not satisfactory compared with other high-performance cathodes. However, coupling LSMCo with BZY can dramatically improve the fuel cell performance, and the performance is the highest ever reported for LSM-based H-SOFCs. Compared with the traditional LSM–BZY composite cathode, the LSMCo–BZY composite cathode has a more active interface with decreased E_{Vo} and reduced distance between Mn 3d and O 2p, benefiting the cathode reaction. As a result, the enhancement by changing the cathode from the LSMCo single-phase cathode to the LSMCo–BZY composite cathode is around 100%, whereas the enhancement is only about 20% for the traditional LSM–BZY composite cathode. In addition, the LSMCo material maintains good chemical stability under both CO_2 and steam conditions, allowing the stable operation of the cell with the LSMCo–BZY cathode for more than 200 h without obvious degradation.

Conflicts of interest

There are no conflicts to declare.

Acknowledgements

This work was supported by the National Natural Science Foundation of China (Grant Number: 51972183) and the Startup Funding for Talents at University of South China.

References

1 Y. Zou, P. C. Tan, B. J. Shi, H. Ouyang, D. J. Jiang, Z. Liu, H. Li, M. Yu, C. Wang, X. C. Qu, L. M. Zhao, Y. B. Fan, Z. L. Wang and Z. Li, *Nat. Commun.*, 2019, **10**, 2695.
2 C. Peng, P. Wei, X. Y. Li, Y. P. Liu, Y. H. Cao, H. J. Wang, H. Yu, F. Peng, L. Y. Zhang, B. S. Zhang and K. L. Lv, *Nano Energy*, 2018, **53**, 97.
3 J. Ma, Y. Kong, S. C. Liu, Y. T. Li, J. B. Jiang, Q. Y. Zhou, Y. S. Huang and S. Han, *ACS Appl. Energy Mater.*, 2020, **3**, 11900.
4 J. R. Ling, Y. F. Zhou, W. T. Xu, H. Lin, S. Lu, B. Wang and K. Wang, *J. Adv. Ceram.*, 2020, **9**, 45.
5 C. X. Duan, Y. Yu, J. Xiao, X. L. Zhang, L. B. Li, P. F. Yang, J. L. Wu and H. X. Xi, *Sci. China Mater.*, 2020, **63**, 667.

6 D. J. L. Brett, A. Atkinson, N. P. Brandon and S. J. Skinner, *Chem. Soc. Rev.*, 2008, **37**, 1568–1578.
7 Y. Zhang, B. Chen, D. Q. Guan, M. G. Xu, R. Ran, M. Ni, W. Zhou, R. O'Hayre and Z. P. Shao, *Nature*, 2021, **591**, 246.
8 E. Wachsman, T. Ishihara and J. Kilner, *MRS Bull.*, 2014, **39**, 773–782.
9 H. K. Dai, H. N. Kou, H. Q. Wang and L. Bi, *Electrochem. Commun.*, 2018, **96**, 11–15.
10 D. Cao, M. Y. Zhou, X. M. Yan, Z. J. Liu and J. Liu, *Electrochem. Commun.*, 2021, **125**, 106986.
11 D. A. Medvedev, J. G. Lyagaeva, E. V. Gorbova, A. K. Demin and P. Tsiakaras, *Prog. Mater. Sci.*, 2016, **75**, 38–79.
12 C. C. Duan, R. J. Kee, H. Y. Zhu, C. Karakaya, Y. C. Chen, S. Ricote, A. Jarry, E. J. Crumlin, D. Hook, R. Braun, N. P. Sullivan and R. O'Hayre, *Nature*, 2018, **557**, 217.
13 J. Li, C. Wang, X. F. Wang and L. Bi, *Electrochem. Commun.*, 2020, **112**, 106672.
14 M. Chen, X. B. Xie, J. H. Guo, D. C. Chen and Q. Xu, *J. Mater. Chem. A*, 2020, **8**, 12566.
15 M. Chen, D. C. Chen, K. Wang and Q. Xu, *J. Alloys Compd.*, 2019, **781**, 857.
16 Y. S. Song, Y. B. Chen, W. Wang, C. Zhou, Y. J. Zhong, G. M. Yang, W. Zhou, M. L. Liu and Z. P. Shao, *Joule*, 2019, **3**, 2842–2853.
17 X. Xu, Y. S. Xu, J. M. Ma, Y. R. Yin, M. Fronzi, X. F. Wang and L. Bi, *J. Power Sources*, 2021, **489**, 229486.
18 Y. D. Zhang, A. K. Zhu, Y. M. Guo, C. C. Wang, M. Ni, H. Yu, C. H. Zhang and Z. P. Shao, *Appl. Energy*, 2019, **238**, 344–350.
19 E. H. Da'as, L. Bi, S. Boulfrad and E. Traversa, *Sci. China Mater.*, 2018, **61**, 57–64.
20 K. Bae, D. Y. Jang, H. J. Choi, D. Kim, J. Hong, B. K. Kim, J. H. Lee, J. W. Son and J. H. Shim, *Nat. Commun.*, 2017, **8**, 14553.
21 L. Bi, S. P. Shafi, E. H. Da'as and E. Traversa, *Small*, 2018, **14**, 1801231.
22 A. P. Tarutin, J. G. Lyagaeva, D. A. Medvedev, L. Bi and A. A. Yaremchenko, *J. Mater. Chem. A*, 2021, **9**, 154–195.
23 H. P. Ding, W. Wu, C. Jiang, Y. Ding, W. J. Bian, B. X. Hu, P. Singh, C. J. Orme, L. C. Wang, Y. Y. Zhang and D. Ding, *Nat. Commun.*, 2020, **11**, 1907.
24 Y. H. Ling, T. M. Guo, Y. Y. Guo, Y. Yang, Y. F. Tian, X. X. Wang, X. M. Ou and P. Z. Feng, *J. Adv. Ceram.*, 2021, **10**, 1052–1060.
25 Y. Xie, N. Shi, D. M. Huan, W. Z. Tan, J. F. Zhu, X. S. Zheng, H. B. Pan, R. R. Peng and C. R. Xia, *ChemSusChem*, 2018, **11**, 3423–3430.
26 Q. Wang, J. Hou, Y. Fan, X. A. Xi, J. Li, Y. Lu, G. Huo, L. Shao, X. Z. Fu and J. L. Luo, *J. Mater. Chem. A*, 2020, **8**, 7704–7712.
27 R. Z. Ren, Z. H. Wang, X. G. Meng, X. H. Wang, C. M. Xu, J. S. Qiao, W. Sun and K. N. Sun, *ACS Appl. Energy Mater.*, 2020, **3**, 4914–4922.
28 Y. Chen, S. Yoo, K. Pei, D. C. Chen, L. Zhang, B. deGlee, R. Murphy, B. T. Zhao, Y. X. Zhang, Y. Chen and M. L. Liu, *Adv. Funct. Mater.*, 2018, **28**, 1704907.
29 Z. R. Tao, X. Xu and L. Bi, *Electrochem. Commun.*, 2021, **129**, 107072.
30 C. Graves, S. D. Ebbesen, S. H. Jensen, S. B. Simonsen and M. B. Mogensen, *Nat. Mater.*, 2015, **14**, 239–244.
31 C. C. Wang, S. Darvish, K. F. Chen, B. X. Hou, Q. Zhang, Z. X. Tan, Y. Zhong and S. Jiang, *Electrochim. Acta*, 2019, **312**, 202–212.
32 J. A. Kilner and M. Burriel, *Annu. Rev. Mater. Res.*, 2014, **44**, 365–393.
33 J. Parbey, Q. Wang, J. L. Lei, M. Espinoza-Andaluz, F. Hao, Y. Xiang, T. S. Li and M. Andersson, *Int. J. Hydrogen Energy*, 2020, **45**, 6949–6957.
34 C. Peng, J. Melnik, J. X. Li, J. L. Luo, A. R. Sanger and K. T. Chuang, *J. Power Sources*, 2009, **190**, 447–452.
35 E. Fabbri, D. Pergolesi and E. Traversa, *Chem. Soc. Rev.*, 2010, **39**, 4355–4369.
36 C. Chen, X. T. Wang, J. H. Zhong, J. L. Liu, G. I. N. Waterhouse and Z. Q. Liu, *Angew. Chem., Int. Ed.*, 2021, **60**, 22043–22050.
37 J. Mei, G. A. Ayoko, C. F. Hu, J. M. Bell and Z. Q. Sun, *Sustainable Mater. Technol.*, 2020, **25**, e00156.
38 J. Mei, T. Liao, J. Liang, Y. X. Qiao, S. X. Dou and Z. Q. Sun, *Adv. Energy Mater.*, 2020, **10**, 1901997.
39 Z. Q. Sun, T. Liao, W. X. Li, Y. X. Qiao and K. Ostrikov, *Adv. Funct. Mater.*, 2019, **29**, 1901460.
40 Y. W. Zhang, J. Mei, C. Yan, T. Liao, J. Bell and Z. Q. Sun, *Adv. Mater.*, 2020, **32**, 1902806.
41 Q. Q. Ji, X. Xu, X. H. Liu and L. Bi, *Electrochem. Commun.*, 2021, **124**, 106964.
42 Y. P. Xia, Z. Z. Jin, H. Q. Wang, Z. Gong, H. L. Lv, R. R. Peng, W. Liu and L. Bi, *J. Mater. Chem. A*, 2019, **7**, 16136–16148.
43 X. H. Zhang, C. L. Pei, X. Chang, S. Chen, R. Liu, Z. J. Zhao, R. T. Mu and J. L. Gong, *J. Am. Chem. Soc.*, 2020, **142**, 11540–11549.
44 A. B. Munoz-Garcia, M. Tuccillo and M. Pavone, *J. Mater. Chem. A*, 2017, **5**, 11825–11833.
45 L. He, Y. Xuan, F. Zhang, X. Wang, H. Q. Pan, J. F. Ren and M. N. Chen, *Int. J. Hydrogen Energy*, 2021, **46**, 1096–1105.
46 W. Y. Liu, H. N. Kou, X. F. Wang, L. Bi and X. S. Zhao, *Ceram. Int.*, 2019, **45**, 20994–20998.
47 Z. W. Zhu, J. Qian, Z. T. Wang, J. J. Dang and W. Liu, *J. Alloys Compd.*, 2013, **581**, 832–835.
48 H. L. Dai, E. H. Da'as, S. P. Shafi, H. Q. Wang and L. Bi, *J. Eur. Ceram. Soc.*, 2018, **38**, 2903.
49 Y. Zheng, Y. F. Li, T. Wu, W. Q. Zhang, J. X. Zhu, Z. P. Li, J. Chen, B. Yu, J. C. Wang and J. J. Zhang, *Nano Energy*, 2018, **51**, 711.
50 D. Gryaznov, R. Merkle, E. A. Kotomin and J. Maier, *J. Mater. Chem. A*, 2016, **4**, 13093–13104.
51 X. K. Lu, X. Yang, L. C. Jia, B. Chi, J. Pu and J. Li, *Int. J. Hydrogen Energy*, 2019, **44**, 16359–16367.
52 Y. S. Xu, X. H. Liu, N. Cao, X. Xu and L. Bi, *Sustainable Mater. Technol.*, 2021, **27**, e00229.
53 W. T. Hong, K. A. Stoerzinger, Y. L. Lee, L. Giordano, A. Grimaud, A. M. Johnson, J. Hwang, E. J. Crumlin, W. L. Yang and Y. Shao-Horn, *Energy Environ. Sci.*, 2017, **10**, 2190–2200.

54 X. B. Zhou, X. B. Liao, X. L. Pan, M. Y. Yan, L. He, P. J. Wu, Y. Zhao, W. Luo and L. Q. Mai, *Nano Energy*, 2021, **83**, 105748.
55 K. C. Lee, M. B. Choi, D. K. Lim, B. Singh and S. J. Song, *J. Power Sources*, 2013, **232**, 224–233.
56 D. K. Lim, H. N. Im, B. Singh and S. J. Song, *J. Electrochem. Soc.*, 2015, **162**, F547–F554.
57 H. L. Dai, X. Xu, C. Liu, C. J. Ma, Q. F. Zhang and L. Bi, *J. Mater. Chem. A*, 2021, **9**, 12553–12564.
58 S. Wu, X. Xu, X. M. Li and L. Bi, *Sci. China Mater.*, 2021, DOI: 10.1007/s40843-021-1821-4.